Available online at www.sciencedirect.com
SCIENCE DIRECT®
Neuroscience Letters 382 (2005) 269–274
Neuroscience Letters
www.elsevier.com/locate/neulet

Voxel-based morphometry to discriminate early Alzheimer's disease from controls

Yoko Hirata[a,d], Hiroshi Matsuda[a,b,*], Kiyotaka Nemoto[a,c], Takashi Ohnishi[a], Kentaro Hirao[a], Fumio Yamashita[c], Takashi Asada[c], Satoshi Iwabuchi[d], Hirotsugu Samejima[d]

[a] *Department of Radiology, National Center Hospital for Mental, Nervous and Muscular Disorders, National Center of Neurology and Psychiatry, 4-1-1 Ogawahigashi, Kodaira, Tokyo 187-8551, Japan*
[b] *Department of Nuclear Medicine, Saitama Medical School, 38 Morohongo, Moroyama-machi, Iruma-gun, Saitama 350-0495, Japan*
[c] *Department of Neuropsychiatry, Institute of Clinical Medicine, University of Tsukuba, 1-1-1 Tennoudai, Tsukuba, Ibaraki, 305-0006, Japan*
[d] *Department of Neurosurgery, Toho Ohashi Hospital, 2-17-6 Ohashi, Meguro, Tokyo 153-8515, Japan*

Received 23 December 2004; received in revised form 18 February 2005; accepted 13 March 2005

Abstract

We assessed the accuracy of voxel-based morphometry (VBM) using a three-dimensional T1-weighted MRI in discriminating Alzheimer's disease (AD) in the very early stage of amnestic type of mild cognitive impairment and age-matched healthy controls. We randomly divided these subjects into two groups. The first group comprising 30 AD patients and 41 controls was used to identify the area with the most significant gray matter loss in patients compared to normal controls based on the voxel-based analysis of a group comparison. The second group comprising 31 patients and 41 controls was used to determine the discrimination accuracy of VBM. A Z-score map for a gray matter image of a subject was obtained by comparison with mean and standard deviation gray matter images of the controls for each voxel after anatomical standardization and voxel normalization to global mean using the following equation; Z-score = ([control mean] − [individual value])/(control S.D.). Receiver operating characteristic curves for a Z-score in the bilateral medial temporal areas including the entorhinal cortex with the most significant loss in the first group showed a high discrimination accuracy of 87.8%. This result would open up a possibility for early diagnosis of AD using VBM.

Keywords: MRI; Alzheimer's disease; Voxel-based morphometry; Mild cognitive impairment

The fact that recently available medications like cholinesterase inhibitors delay the progression of Alzheimer's disease (AD) has increased the urgency of diagnosing AD at an early stage. Numerous structural MRI studies have demonstrated that atrophy of the medial temporal lobe, including the hippocampus and entorhinal cortex, is a sensitive marker of early AD [6,15]. Moreover it has been suggested that atrophy of medial temporal lobe structures might predict progression from mild cognitive impairment (MCI) to AD [16,25]. Of medial temporal lobe structures, it has been argued that decreased entorhinal cortex volume might be a particularly sensitive predictor of AD on the basis of tangle deposition of early entorhinal cortex involvement in AD with subsequent spread to the hippocampus proper [3]. Killiany et al. [16] used MRI to measure the volumes of the entorhinal cortex and hippocampus in 137 individuals, and found that the volume of the entorhinal cortex distinguished the subjects who were destined to develop dementia with considerable accuracy, whereas the hippocampus measure did not.

However, it is difficult to evaluate atrophy of the entorhinal cortex by visual inspection. On the other hand, volumetric

* Corresponding author. Tel.: +81 49 276 1302; fax: +81 49 276 1301.
E-mail address: matsudah@saitama-med.ac.jp (H. Matsuda).

0304-3940/$ – see front matter © 2005 Elsevier Ireland Ltd. All rights reserved.
doi:10.1016/j.neulet.2005.03.038

assessment of the entorhinal cortex in routine clinical practice requires the very time-consuming nature of region of interest analysis, which is dependent on the expertise of the tracers and lacks an automated volume measurement technique. Recently a new automated method of measuring brain atrophy has been developed [2,21]. This new method of voxel-based morphometry (VBM) objectively maps gray matter loss on a voxel-by-voxel basis after anatomical standardization analogous to that used in functional neuroimaging. The advantage of VBM over analyses based on region of interest is that VBM produces an unbiased result from exploration of the whole brain. This approach has been reported to show higher accuracy of discriminating AD and controls than region of interest-based analysis [24]. The present VBM study was undertaken to evaluate the ability to discriminate very early AD patients from age-matched controls using a newly developed software program.

We retrospectively chose 61 patients (32 men and 29 women) with a clinical diagnosis of probable AD patients according to the National Institute of Neurological and Communicative Disorders and Stroke and the Alzheimer's Disease and Related Disorders Association criteria (NINCDS-ADRDA) [18]. At the initial visit, they showed verbal and/or visual episodic memory impairment in delayed recall, as defined by performance 1.5S.D. below the mean for age-matched normal controls in learning of a list of 10 words, 15-item story recall test, and Rey–Osterrieth complex figure test [12]. They had no apparent loss in general cognitive, behavioral, or functional status and corresponded to the criteria of amnestic type of MCI proposed by Petersen et al. [22] or 0.5 in Clinical Dementia Rating [13]. They ranged in age from 48 to 87 years with a mean ± S.D. of 70.6 ± 8.4. The Mini-Mental State Examination (MMSE) [8] score ranged from 24 to 29; 26.0 ± 1.5 at the initial visit. During the subsequent follow-up period of two to six years, the subjects showed progressive cognitive decline and eventually fulfilled the diagnosis of probable AD according to the NINCDS-ADRDA.

Eighty-two control subjects (39 men and 43 women, age; 54–86 years, mean 70.1, S.D. 7.7) were healthy volunteers with no memory impairment or cognitive disorders. Their performance was within normal limits both on the Wechsler Memory Scale—Revised and Wechsler Adult Intelligence Scale—Revised. The MMSE score ranged from 26 to 30; 28.7 ± 1.5. They did not differ significantly in age or education from the AD patients. The Ethics Committee of the National Center of Neurology and Psychiatry approved this study for healthy volunteers, all of whom provided informed consent to participate.

All of the subjects were right handed and screened by questionnaire and medical history to exclude those with medical conditions potentially affecting the central nervous system. In addition, none of them had asymptomatic cerebral infarction detected by T2-weighted MRI.

All MRI studies were performed on a 1.0-T system (Magnetom Impact Expert, Siemens, Erlangen, Germany). A three-dimensional volumetric acquisition of a T1-weighted gradient echo sequence produced a gapless series of thin sagittal sections using an MPRage sequence (echo time/repetition time, 4.4/11.4; flip angle, 15°; acquisition matrix, 256 × 256; 1 excitation; field of view, 31.5 cm; slice thickness, 1.23 mm).

The VBM for an MR image was performed as described in our previous study [17] based on the method proposed by Baron et al. [2]. The theory and algorithm of this VBM were well-documented by Ashburner and Friston [1]. The acquired MR images were reformatted to gapless 2-mm-thick transaxial images. Images were analyzed using Statistical Parametric Mapping 2002 (SPM2) (Wellcome Department of Imaging Neuroscience, London, UK) running on MATLAB (The MathWorks, Inc., Sherborn, MA, USA). Anatomical standardization fitted each individual brain to a standard template brain (Talairach and Tournoux [23]) in three-dimensional space, so as to correct for differences in brain size and shape and facilitate intersubject averaging. In the first anatomical standardization, only 12-parameter affine transformation was used. Normalized MR images were then segmented into gray matter, white matter, cerebrospinal fluid, and other compartments using a modified version of the clustering algorithm, the maximum likelihood "mixture model" algorithm. The segmentation procedure involves calculating for each voxel a Bayesian probability of belonging to each tissue class based on a priori MRI information with a non-uniformity correction. The segmented gray matter images were then subjected to an affine and non-linear anatomical standardization using a template of a priori gray matter. The anatomically standardized gray matter images were smoothed with an isotropic Gaussian kernel 12 mm in full width at half maximum (FWHM) to use the partial volume effect to create a spectrum of gray matter intensities. The gray matter intensities are equivalent to the weighted average of gray matter voxels located in the volume fixed by the smoothing kernel. Regional intensities can therefore be taken as equivalent to gray matter concentration [1].

We randomly selected 30 patients and 41 healthy volunteers as the first group to establish the region with the most significant decline of gray matter concentrations in patients using SPM2. The patients and healthy volunteers were compared using the "compare-population one scan/subject" routine in SPM2. The "proportional scaling" routine was used to control for individual variation in global mean intensities. The resulting set of values for each contrast constituted a statistical parametric map of the t-statistic SPM$\{t\}$. The SPM$\{t\}$ were transformed to the unit normal distribution {SPM(Z)} and thresholded at $P < 0.001$. The significance of each region was estimated with a threshold of $P = 0.01$ with correction for multiple non-independent comparisons. Extent threshold was set to 0 voxels.

A software program running on Windows XP for analysis of gray matter images was newly developed to discriminate between the remaining 31 patients and 41 healthy volunteers as the second group. Each gray matter image of the patients was compared to the mean and S.D. of gray matter images

of the 41 healthy volunteers using voxel-by-voxel Z-score analysis after voxel normalization to global mean intensities; Z-score = ([control mean] − [individual value])/(control S.D.) as previously reported by Minoshima et al. in a PET study [20]. These Z-score maps were displayed by overlay on tomographic sections. We designated this software program as the voxel-based specific region analysis for Alzheimer's disease (VSRAD) which can automatically analyze three-dimensional T1-weighted MRI data as a series of segmentation, anatomical standardization and smoothing using SPM2 without a Matlab program, and Z-score analysis. This program registered the SPM{t} results for significant decline of gray matter concentrations in patients determined by group comparison in the first group as a specific region of interest.

Each gray matter image of one of the 41 healthy volunteers was also compared with the averaged gray matter image of the remaining 40 healthy volunteers in the same manner as in the patients. Using the averaged value of positive Z-scores in the specific region of interest in a Z-score map as the threshold, receiver operating characteristic (ROC) curves were determined using the ROCKIT 0.9β and the PlotROC programs developed by Metz et al. (http://xray.bsd.uchicago.edu/krl) [19]. The program calculates the area under the ROC curves (Az), accuracy, sensitivity and specificity. Accuracy was determined as the value at the point where the sensitivity is the same as the specificity on the ROC curve.

The SPM2 analysis demonstrated significant declines of gray matter concentrations of patients only in the left (−17, −8, −18, x, y, z; $Z = 5.47$) and the right (16, −9, −18, x, y, z; $Z = 5.42$) parahippocampal gyri in the first group (Fig. 1). These regions correspond to Brodmann areas 28 (entorhinal area) and 34 (dorsal entorhinal area) and constitute the entire entorhinal area together [4]. These regions of bilateral parahippocampal areas are delineated as specific regions of interest for very early AD.

Then the averaged value of positive Z-scores in these bilateral specific regions of interest was obtained in a Z-score map (Fig. 2) in the second group using a VSRAD software program. Using these averaged Z-score values in these specific regions of interest the ROC curves for discrimination of patients from healthy volunteers were computed (Fig. 3). The Az and accuracy were 0.949 (95% confidence interval 0.880–0.982) and 87.8%, respectively.

In the present study, automated voxel-based analysis using a Z-score value in the bilateral medial temporal areas including the entorhinal cortex after anatomical standardization of gray matter images revealed a high accuracy of 87.8% in the discrimination of AD patients in the very early stage

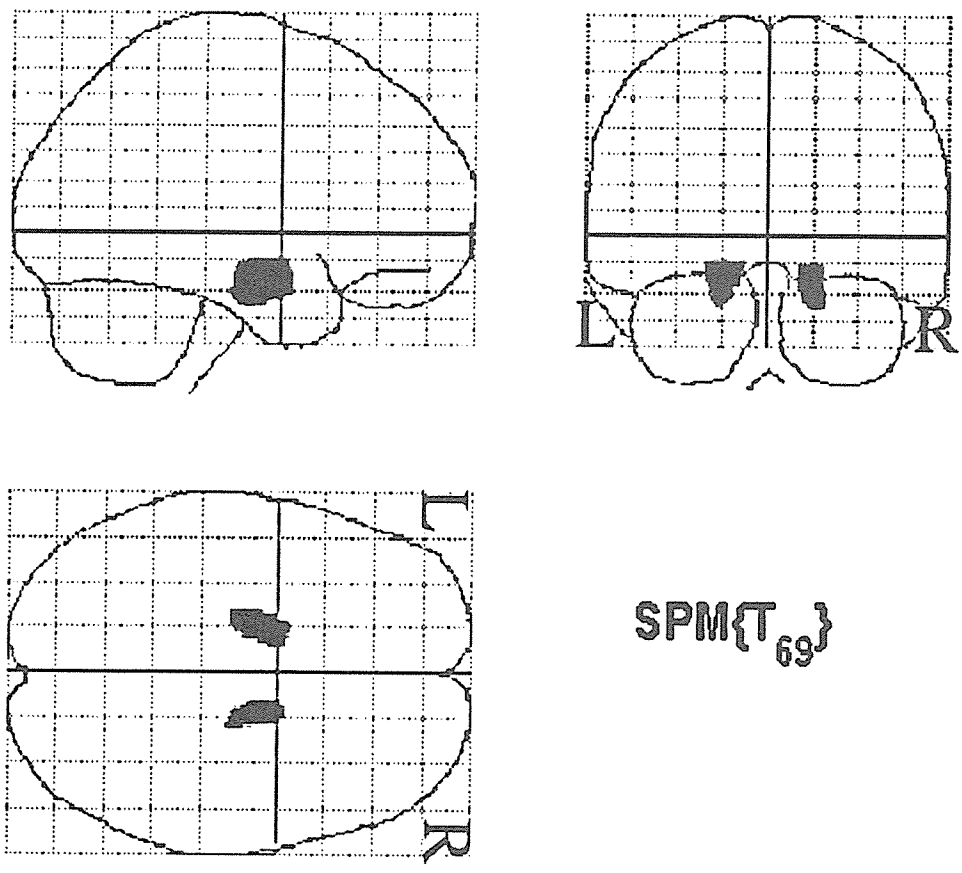

Fig. 1. Maximum intensity projections of SPM2 results for significant decline of gray matter concentration in very early AD patients as compared with age-matched healthy volunteers (−17, −8, −18, x,y,z; $Z = 5.47$; 16, −9, −18, x,y,z; $Z = 5.42$). These regions correspond to bilateral Brodmann areas 28 and 34. Height threshold <0.001, corrected for multiple comparisons.

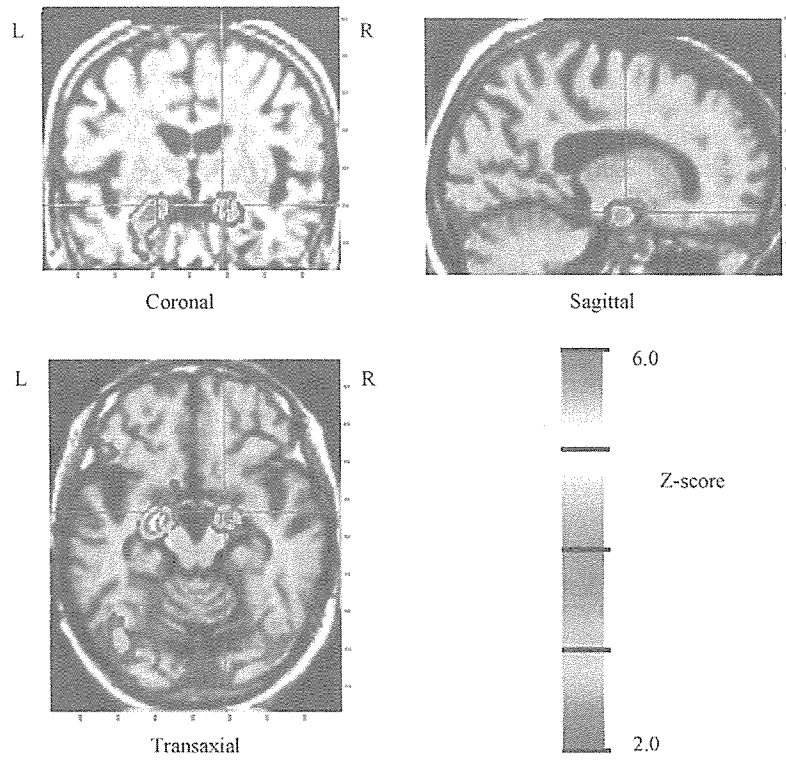

Fig. 2. Automated voxel-by-voxel Z-score analysis by comparison of a gray matter image for an 82-year-old woman at the stage of MCI before conversion to AD with MMSE of 24 with the mean and standard deviation gray matter images of healthy volunteers after normalization to global mean voxel intensities. The color-scaled Z-score maps ranging from 2.0 to 6.0 were displayed by overlaying on orthogonal sections of the anatomically standardized MRI of the patient. Red lines enclose areas with the most significant decline of gray matter concentration in very early AD obtained from group comparison with healthy volunteers by SPM2. The averaged value of positive Z-scores in this specific region is 2.4.

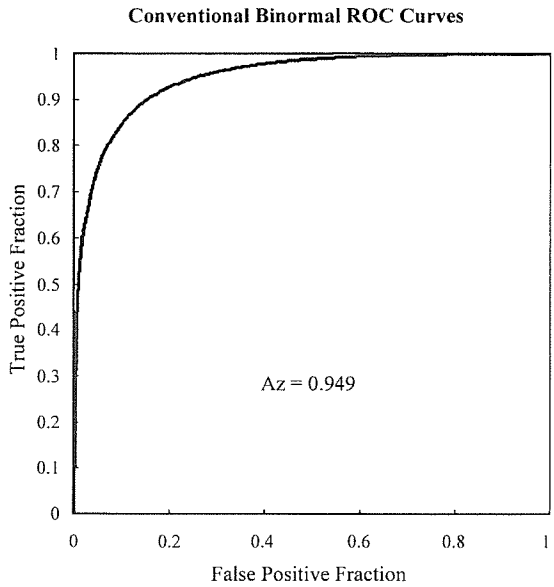

Fig. 3. Receiver operating characteristic (ROC) curves for discrimination between probable AD patients at the very early stage of amnestic MCI and healthy volunteers when thresholding at the averaged values of positive Z-scores in the medial temporal areas including the entorhinal cortex. The Az and accuracy were 0.949 and 87.8%, respectively.

from healthy volunteers. We adopted the VBM procedure proposed by Baron et al. [2] in which segmentation of the MR images based on an affine only and reversible normalization was followed by the full spatial normalization process with both affine transform and non-linear warping only onto the segmented gray matter set based on the standard gray matter template. Presumably because of segmentation errors due to partial volume effects inherently created by warping, the use of standard full normalization prior to segmentation appears to increase the risk of misclassification of non-brain tissue as gray matter voxels.

Neuropathological studies have provided detailed information about which specific brain regions are selectively affected in the earliest stage of AD. The initial neuronal lesions of the neurofibrillary tangles and neuritic plaques appear to occur in the entorhinal cortex, a portion of the anterior parahippocampal gyrus that receives projections from widespread limbic and association areas and gives rise to the perforant pathway, the major cortical excitatory input to the hippocampus itself [10,14]. Some layers of the entorhinal cortex undergo 40–60% neuronal depopulation even in the earliest phase of AD, when memory impairments and patient complaints are subtle and the symptoms do not reach the threshold for a diagnosis of AD [10]. In the present VBM study, SPM2 revealed gray matter loss selectively in the bilateral medial

temporal areas including entorhinal areas in very early AD in good agreement with these pathological changes in the amnestic stage of AD. Frisoni et al. [9] reported the most significant gray matter loss in bilateral hippocampal/amygdalar complex using SPM99 in three very early AD patients with MMSE scores of over 24. Using SPM99, Chetelat et al. [5] also reported significant gray matter loss predominantly affecting the hippocampal region and cingulate gyri in patients with amnestic MCI.

A method for automated diagnosis of gray matter loss was developed in the present study. In this software program, voxel-based analysis was performed using a Z-score map calculated from comparison of a patient's data with the control database. This program has the advantage of being able to incorporate SPM2 results into automated analysis of Z-score values as a specific region of interest. The specific region of interest can be determined by group comparison of gray matter images for patients with a neuropsychiatric disease with those for healthy volunteers using SPM2. Herholtz et al. [11] developed a similar original software program based on an automated voxel-based procedure after anatomical image standardization for discrimination between probable AD and controls using ^{18}F-fluorodeoxyglucose PET. They reported 84% sensitivity and 93% specificity for discrimination between very mild probable AD with MMSE over 24 and controls. The current VBM study on very mild probable AD provided almost the same accuracy as that in a PET study.

Finally we must refer to several study limitations. First, the sample size is too small to conclude whether this VBM approach to early diagnosis of AD is truly useful for a routine clinical MRI study or not. If this approach is extended to a multi-center study for a larger sample size, we have to resolve the systematic variations in raw original structural images obtained from different MR scanners. Second, we investigated amnestic MCI patients who all converted to AD. The outcome for any patient with MCI is uncertain because many subjects may remain stable or ever revert to a normal state, while others progress to dementia. Accordingly the predictive study using this VBM approach is much more important for MCI conversion to AD. Third, although the present cross-sectional study provided high discrimination accuracy between AD and controls, it has been reported that longitudinal measures of the annual atrophy rate of the entorhinal cortex elevated the discrimination accuracy of early AD and controls from 77% for the cross-sectional baseline study to 82% [7]. This fully automated software with incorporation of a specific region for longitudinal changes in very early AD would be expected to enhance the discrimination accuracy of VBM in follow-up studies. Fourth, VBM does not have the anatomical precision attainable by classic ROI-based volumetric studies. This is because of the need to anatomically standardize and smooth the data in order to reduce the effect of intersubject differences in normal gyral anatomy and in turn to allow for a statistical, voxelwise analysis across subjects. However, this limitation should not detract from the considerable advantages of the voxel-based analysis in terms of efficiency, comprehensiveness, and freedom from observer bias.

In conclusion, an automated analysis of VBM using a Z-score map was applied to discrimination between probable AD patients at the very early stage of amnestic MCI and age-matched healthy volunteers. ROC analysis of the averaged value of positive Z-scores in the bilateral medial temporal areas including the entorhinal cortex for the very early stage of probable AD determined by SPM2 demonstrated discrimination accuracy of 87.8%. The VBM would thus lead to the possibility for the early diagnosis of AD in an MRI study.

Acknowledgments

We are very thankful to the technical staff in our hospital for data acquisition of MRI, and Mr. John Gelblum for his proofreading of this manuscript.

References

[1] J. Ashburner, K.J. Friston, Voxel-based morphometry—the methods, Neuroimage 11 (2000) 805–821.
[2] J.C. Baron, G. Chetelat, B. Desgranges, G. Perchey, B. Landeau, V. De. La. Sayette, F. Eustache, In vivo mapping of gray matter loss with voxel-based morphometry in mild Alzheimer's disease, Neuroimage 14 (2001) 298–309.
[3] H. Braak, E. Braak, Evolution of the neuropathology of Alzheimer's disease, Acta Neurol. Scand. Suppl. 165 (1996) 3–12.
[4] K. Brodmann, Vergleichende Lokalisationslehre der Groshirnrinde, Barth, Leipzig, 1925.
[5] G. Chetelat, B. Desgranges, V. De. La. Sayette, F. Viader, F. Eustache, J.C. Baron, Mapping gray matter loss with voxel-based morphometry in mild cognitive impairment, NeuroReport 13 (2002) 1939–1943.
[6] A.T. Du, N. Schuff, D. Amend, M.P. Laakso, Y.Y. Hsu, W.J. Jagust, B.L. Miller, B.R. Reed, D. Mungas, K. Yaffe, H.C. Chui, M.W. Weiner, Magnetic resonance imaging of the entorhinal cortex and hippocampus in mild cognitive impairment and Alzheimer's disease, J. Neurol. Neurosurg. Psychiatry 71 (2001) 441–447.
[7] A.T. Du, N. Schuff, X.P. Zhu, W.J. Jagust, B.L. Miller, B.R. Reed, J.H. Kramer, D. Mungas, K. Yaffe, H.C. Chui, M.W. Weiner, Atrophy rates of entorhinal cortex in AD and normal aging, Neurology 60 (2003) 481–486.
[8] M.F. Folstein, S.E. Folstein, P.R. McHugh, Mini-Mental State: a practical method for grading the cognitive state of patients for the clinician, J. Psychiatr. Res. 12 (1975) 189–198.
[9] G.B. Frisoni, C. Testa, A. Zorzan, F. Sabattoli, A. Beltramello, H. Soininen, M.P. Laakso, Detection of grey matter loss in mild Alzheimer's disease with voxel based morphometry, J. Neurol. Neurosurg. Psychitatry 73 (2002) 657–664.
[10] T. Gomez-Isla, J.L. Price, D.W. McKeel Jr., J.C. Morris, J.H. Growdon, B.T. Hyman, Profound loss of layer II entorhinal cortex neurons occurs in very mild Alzheimer's disease, J. Neurosci. 16 (1996) 4491–4500.
[11] K. Herholz, E. Salmon, D. Perani, J.C. Baron, V. Holthoff, L. Frolich, P. Schonknecht, K. Ito, R. Mielke, E. Kalbe, G. Zundorf, X. Delbeuck, O. Pelati, D. Anchisi, F. Fazio, N. Kerrouche, B. Desgranges, F. Eustache, B. Beuthien-Baumann, C. Menzel, J. Schroder, T. Kato, Y. Arahata, M. Henze, W.D. Heiss, Discrimination between Alzheimer dementia and controls by automated analysis of multicenter FDG PET, Neuroimage 17 (2002) 302–316.

[12] J.R. Hodges, Cognitive Assessment for Clinicians, Oxford Medical Publications, Oxford, 1993.
[13] C.P. Hughes, L. Berg, W.L. Danziger, L.A. Coben, R.L. Martin, A new clinical scale for the staging of dementia, Br. J. Psychiatry 140 (1982) 566–572.
[14] B.T. Hyman, G.W. Van Hoesen, C. Kromer, A.R. Damasio, Alzheimer's disease: cell specific pathology isolates the hippocampal formation, Science 225 (1984) 1168–1170.
[15] R.J. Killiany, T. Gomez-Isla, M. Moss, R. Kikinis, T. Sandor, F. Jolesz, R. Tanzi, K. Jones, B.T. Hyman, M.S. Albert, Use of structural magnetic resonance imaging to predict who will get Alzheimer's disease, Ann. Neurol. 47 (2000) 430–439.
[16] R.J. Killiany, B.T. Hyman, T. Gomez-Isla, M.B. Moss, R. Kikinis, F. Jolesz, R. Tanzi, K. Jones, M.S. Albert, MRI measures of entorhinal cortex vs hippocampus in preclinical AD, Neurology 58 (2002) 1188–1196.
[17] H. Matsuda, N. Kitayama, T. Ohnishi, T. Asada, S. Nakano, S. Sakamoto, E. Imabayashi, A. Kato, Longitudinal evaluation of both morphologic and functional changes in the same individuals with Alzheimer's disease, J. Nucl. Med. 43 (2002) 304–311.
[18] G. McKhann, D. Drachman, M. Folstein, R. Katzman, D. Prie, E.M. Stadlan, Clinical diagnosis of Alzheimer's disease: Report of the NINCDS-ADRDA work group under the auspices of department of health and human service task force on Alzheimer's disease, Neurology 34 (1984) 939–944.
[19] C.E. Metz, B.A. Herman, C.A. Roe, Statistical comparison of two ROC-curve estimates obtained from partially-paired datasets, Med. Decis. Making 18 (1998) 110–121.
[20] S. Minoshima, K.A. Frey, R.A. Koeppe, N.L. Foster, D.E. Kuhl, A diagnostic approach in Alzheimer's disease using three-dimensional stereotactic surface projections of fluorine-18-FDG PET, J. Nucl. Med. 36 (1995) 1238–1248.
[21] T. Ohnishi, H. Matsuda, T. Tabira, T. Asada, M. Uno, Changes in brain morphology in Alzheimer disease and normal aging: is Alzheimer disease an exaggerated aging process? Am. J. Neuroradiol. 22 (2001) 1680–1685.
[22] R.C. Petersen, R. Doody, A. Kurz, R.C. Mohs, J.C. Morris, P.V. Rabins, K. Ritchie, M. Rossor, L. Thal, B. Winblad, Current concepts in mild cognitive impairment, Arch. Neurol. 58 (2001) 1985–1992.
[23] J. Talairach, P. Tourmoux, Co-Planar Stereotaxic Atlas of the Human Brain, Tieme Medical, New York, 1988.
[24] C. Testa, M.P. Laakso, F. Sabattoli, R. Rossi, A. Beltramello, H. Soininen, G.B. Frisoni, A comparison between the accuracy of voxel-based morphometry and hippocampal volumetry in Alzheimer's disease, J. Magn. Reson. Imaging 19 (2004) 274–282.
[25] P.J. Visser, F.R. Verhey, P.A. Hofman, P. Scheltens, J. Jolles, Medial temporal lobe atrophy predicts Alzheimer's disease in patients with minor cognitive impairment, J. Neurol. Neurosurg. Psychiatry 72 (2002) 491–497.

Available online at www.sciencedirect.com
SCIENCE DIRECT®
Neuroscience Letters 386 (2005) 111–115
Neuroscience Letters
www.elsevier.com/locate/neulet

Immunohistochemical study of the hnRNP A2 and B1 in the hippocampal formations of brains with Alzheimer's disease

Katsuyoshi Mizukami [a,*,1], Masanori Ishikawa [a], Masahiko Iwakiri [a], Milos D. Ikonomovic [b], Steven T. Dekosky [b], Hiroshi Kamma [c], Takashi Asada [a]

[a] *Department of Psychiatry, Institute of Clinical Medicine, University of Tsukuba, 1-1-1 Tennodai, Tsukuba City, Ibaraki 305-8575, Japan*
[b] *Western Psychiatric Institute and Clinic University of Pittsburgh, 3811 O'Hara Street, Pittsburgh, PA 15213, USA*
[c] *Department of Pathology, Institute of Basic Sciences, University of Tsukuba, 1-1-1 Tennodai, Tsukuba city, Ibaraki 305-8575, Japan*

Received 5 April 2005; received in revised form 18 May 2005; accepted 31 May 2005

Abstract

To elucidate the post-transcriptional regulation in the subjects with Alzheimer's disease (AD), we employed immunohistochemical techniques and examined the expression of the heterogeneous nuclear ribonucleoprotein (hnRNP) A2 and B1 in the hippocampus with neurofibrillary tangle (NFT) neuropathology. In the mildly affected subjects (Braak stages I and II), the most intense A2 immunoreactivity was observed in the CA3 to CA1 neurons. In the moderately (Braak stages III and IV) and severely affected subjects (Braak stages V and VI), the CA1 region demonstrated a decrease in the number of A2 immunoreactive neurons and in immunoreactivity in the remaining neurons, while within the CA4 to CA2 in the severely affected subjects, the majority of neurons showed increased A2 immunoreactivity. An intense B1 immunoreactivity was observed throughout the CA subfields. In the CA1 subfield of the moderately affected subjects and in the extensive hippocampal regions of the severely affected subjects, a decrease in B1 immunoreactivity was observed. Double-immunolabeling studies demonstrated that tangle-bearing neurons reduced A2 and B1 immunoreactivity. Our study suggests that hnRNP A2 and B1 display different responses in the AD hippocampus, and further suggests that the post-transcriptional regulation is disturbed in neurons of the AD hippocampus.

Keywords: Alzheimer's disease; Heterogeneous nuclear ribonucleoprotein (hnRNP); Hippocampus; mRNA; Post-transcriptional regulation

Alzheimer's disease (AD) is characterized pathologically by the presence of amyloid beta protein (Aβ) deposits and neurofibrillary tangles (NFT) and the loss of nerve cells and synapses. It is well-documented that certain regions in the hippocampus are prone to developing AD pathology, whereas other regions display a greater resistance. In exploring the molecular basis underlying the selected vulnerability of neurons in the AD brain, we believe it is important to understand the alterations in the transcriptional and post-transcriptional regulation of neurons. Although a growing body of evidence suggests that some pathological incidents in the AD brain are associated with post-transcriptional regulation [1,7,13,21,22], and overall post-transcriptional regulation is reported to be reduced in severely affected subjects with AD [19], the details of the post-transcriptional regulation in AD brain remains unclear. Heterogeneous nuclear ribonucleoprotein (hnRNP) proteins directly bind to pre-mRNA forming a large multiprotein–RNA complex and have important roles in the post-transcriptional regulations, such as the splicing and transport of mRNAs [4,18]. hnRNP A2 and B1 are produced by alternative splicing from a single copy gene [12], and they are one of the most abundant and important nuclear RNA-binding proteins [4]. The expression of these hnRNP proteins may, in part, reflect post-transcriptional regulation [15]. In this study, to elucidate neuronal post-transcriptional regulations, we

* Corresponding author. Tel.: +81 298 53 3210; fax: +81 298 53 3183.
E-mail address: mizukami@md.tsukuba.ac.jp (K. Mizukami).
[1] Tel.: 81 298 53 3182; fax: 81 298 53 3182.

0304-3940/$ – see front matter © 2005 Elsevier Ireland Ltd. All rights reserved.
doi:10.1016/j.neulet.2005.05.070

employed immunohistochemical techniques to examine the alterations in hnRNP A2 and B1 proteins in the hippocampus from elderly subjects with NFT neuropathology.

Postmortem brain tissue was obtained from 17 elderly subjects (Table 1): 13 with a clinical diagnosis of AD (77.7 ± 12.7 years) and 4 age-matched cognitively normal control subjects (73.3 ± 16.5 years). The mean postmortem interval (PMI) and brain weight of the cases were 6.5 ± 4.9 h and 1167 ± 126 g, respectively. For non-demented subjects, clinical evaluations were largely based on retrospective analysis of medical records and interviews with their physicians and immediate family members. AD subjects were all participants in a longitudinal research program maintained by the University of Pittsburgh, Alzheimer's Disease Research Center (ADRC). As participants in this program, patients underwent periodic neuropsychological and neurological evaluation. Clinical diagnosis of AD was based on a standardized ADRC evaluation at a Consensus Conference, utilizing DSM-IV [2] and NINCDS/ADRDA [14] criteria. Neuropathologic diagnosis was based, in part, on histologic examination of brain tissue sections with hematoxylin and eosin, thioflavine-S, and Bielschowsky silver stains. Each case received a severity rating of I–VI according to Braak and Braak [3]. Of the 17 cases, 3 cases were stage I, 1 was stage II, 1 was stage III, 3 were stage IV, there were no cases of stage V, and 9 were stage VI. Because of the small number of subjects within each stage, we grouped subjects into mild (stages I and II, $N=4$), moderate (stages III and IV, $N=4$), and severe (stages V and VI, $N=9$) groups. Of the 13 cases with a clinical diagnosis of AD, the number of subjects belonging to the mild, moderate, and severe groups was 0, 4, and 9, respectively. Likewise, the number of elderly controls belonging to these three groups was 4, 0, and 0, respectively. None of the patients had any other confounding neurological or neuropathologic disorders that interfered with our studies of the hippocampus.

Table 1

Number	Age	Sex	Weight (g)	PMI (h)	Braak stage
Non-demented subjects					
1	61	F	1360	18	I
2	57	F	1400	8	I
3	87	F	1120	8	I
4	88	F	990	5.5	II
AD subjects					
1	91	F	1260	3	III
2	75	M	1300	7	IV
3	81	M	1150	4	IV
4	72	M	1160	4	IV
5	100	F	970	5	VI
6	48	M	1100	8	VI
7	81	F	1130	4	VI
8	86	M	1330	2	VI
9	72	M	1080	4	VI
10	74	M	960	4	VI
11	62	M	1150	4	VI
12	84	F	1070	5	VI
13	89	F	1070	5	VI

Brain tissue was processed according to previously described procedures [9,10,15]. Blocks of tissue containing hippocampus were cut in a coronal plane and placed in 0.1 M phosphate buffer (PB, pH = 7.4) containing 4% paraformaldehyde for 24–48 h at 4 °C and then cryoprotected in 30% sucrose concentration in PB for several days. The tissue was then sectioned at 40 μm on a sliding, freezing microtome. For each case, at least one section was stained for Nissl substance to delineate the cytoarchitectural boundaries of the hippocampus as defined by Duvernoy [5].

The sections were processed for immunocytochemistry as previously described [9,10,15]. Tissue sections were immunocytochemically labeled using an avidin–biotin immunolabeled procedure using 4G8 and 2B2, both of which are raised in mice; 4G8 represents A2 while 2B2 represents B1 [11]. The primary antibodies were diluted 1/1000 for 4G8 and 1/2000 for 2B2 in Tris–saline containing 3% goat serum and 0.25% Triton X-100. At least three sections from each case were used for this study, and sections were processed together to control for any variability in the immunocytochemical procedure. As a control for nonspecific staining, sections were either incubated with initial incubation media minus the primary antibody or processed as described. Furthermore, representative sections were double-labeled using 4G8 or 2B2 and PHF-1 (generously provided by Dr. Peter Davis). PHF-1 recognizes tau protein phosphorylated at serine residues 396 and 404 [17]. Thus, these double-labeling studies allow us to investigate alterations of hnRNP A2 and B1 in neurons with NFT pathlogy. For double-labeling, immediately after the completion of PHF-1 immunohistochemistry, 4G8 or 2B2 immunohistochemistry was performed on the same section. As for chromagens, we used diaminobenzidine for PHF-1, and diaminobenzidine plus 2.5% nickel ammonium sulfate for 4G8 or 2B2, yielding brown and black reaction products, respectively.

Throughout the hippocampus intense A2 immunoreactivity was observed in the nucleoplasm of neurons and weak immunoreactivity was observed in the cytoplasm and proximal dendrites of neurons (Fig. 1A–L). A2 immunoreactivity was observed in the nucleoplasm of glial cells and ependymal cells, but the intensity was weak. In the subjects with mild pathology (Braak stages I and II), we observed an intense A2 immunoreactivity in the neuronal nucleoplasm from the CA3 to CA1 subfield (Fig. 1B–D), while CA4 neurons and the dentate granule cells were less intensely immunoreactive for A2 (Fig. 1A). In the moderately affected subjects (Braak stages III and IV), overall the distribution and intensity of A2 immunoreactivity appeared indistinguishable from that in mild cases (Fig. 1E–G), although the CA1 subfield showed a decrease in the number of A2 immunoreactive neurons and reduced A2 immunoreactivity in the remaining neurons (Fig. 1H). Interestingly, in the severely affected subjects (Braak stages V and VI), within the CA4 to CA2 subfields, the majority of neurons showed increased A2 immunoreac-

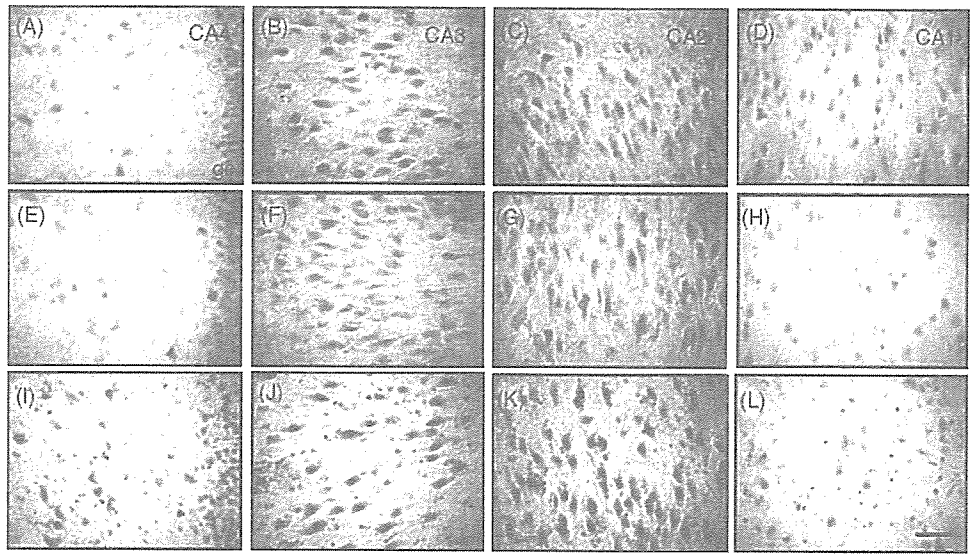

Fig. 1. Photomicrographs showing A2 immunohistochemistry in the hippocampus with mild (A–D), moderate (E–H), and severe (I–L) neurofibrillary pathology. In the mild case, an intense immunoreactivity for A2 was observed in the neuronal nucleoplasm from the CA3 to the CA1 subfield (B–D), while CA4 neurons and the dentate granule cells were less intensely immunoreactive (A). In the moderate case (E–G), overall the distribution and intensity of A2 immunoreactivity appeared indistinguishable from that in the mild cases, although the CA1 subfield showed a decrease in the number of A2 immunoreactive neurons and a reduction of A2 immunoreactivity in the remaining neurons (H). In the severely affected case, within the CA4 to CA2 subfields, the majority of neurons showed increased A2 immunoreactivity (I–K), while CA1 neurons maintained decreased A2 immunoreactivity (L). Bar = 50 μm. gc, granular cell.

tivity (Fig. 1I–K), while CA1 neurons maintained decreased A2 immunoreactivity (Fig. 1L).

In contrast to A2 immunoreactivity, immunoreactivity for B1 was observed exclusively in the nucleoplasm of neurons, in glial cells as well as ependymal cells, and it was not detected in the neuronal cytoplasm (Fig. 2A–L). An intense immunoreactivity for B1 was observed throughout the CA subfields, although in the granule cells, B1 immunoreactivity was relatively weak (Fig. 2A). In the moderately affected subjects, the pattern of B1 immunoreactivity was indistinguishable from that in the mild cases (Fig. 2E–G), although within the CA1 subfield we observed a decrease in the number of B1 immunoreactive neurons (Fig. 2H). In the severely affected subjects, within the CA4 to CA2 subfields neurons

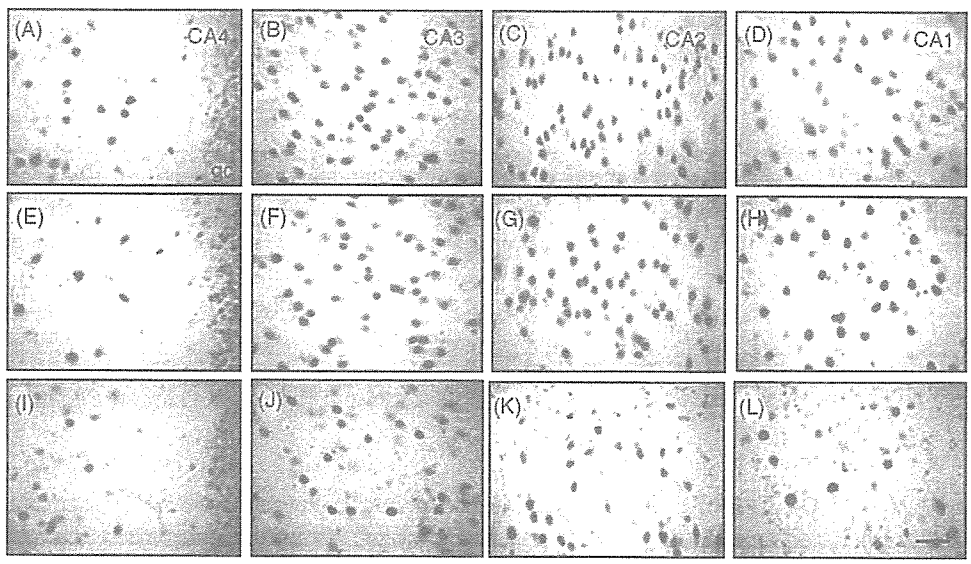

Fig. 2. Photomicrographs showing B1 immunohistochemistry in the hippocampus with mild (A–D), moderate (E–H), and severe (I–L), neurofibrillary pathology. In the mildly affected case, an intense immunoreactivity for B1 was observed throughout the CA subfields, although in the granule cells, B1 immunoreactivity was relatively weak (A). In the moderately affected case, the pattern of B1 immunoreactivity was indistinguishable from that in the mild cases (E–G), although within the CA1 subfield the number of B1 immunoreactive neurons was reduced (H). In the severely affected case, a decrease in B1 immunoreactivity was observed within the CA4 to CA2 subfields (I–K), and in the CA1 subfield, only a few neurons showed an intense immunoreactivity for B1 (L). Bar = 50 μm. gc, granular cell.

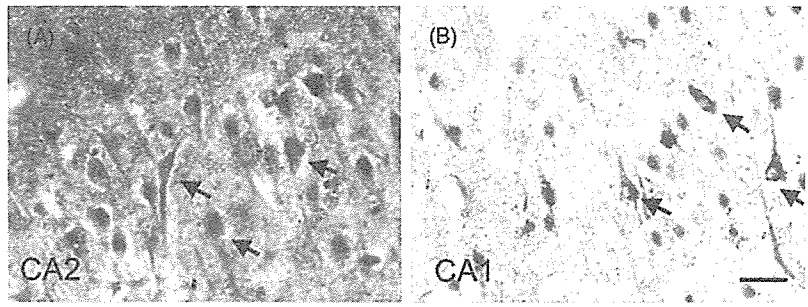

Fig. 3. Photomicrographs showing double-immunolabeling with PHF-1 (Fig. 2A and B, brown) and A2 (Fig. 2A, grey) or B1 (Fig. 2B, grey). PHF1-positive neurons often had reduced A2 and B1 immunoreactivity (black arrows). Bar = 50 μm.

often reduced B1 immunoreactivity (Fig. 2I–K), and in the CA1 subfield, only a few neurons showed immunoreactivity for B1 (Fig. 2L).

Double-immunolabeling study demonstrated that the majority of PHF1-positive neurons had reduced or lost A2 (Fig. 3A) and B1 (Fig. 3B) immunoreactivity, although we still observed intense immunoreactivity for A2 and B1 in some PHF1-positive neurons.

This is the first paper reporting A2 and B1 immunohistochemistry in the human hippocampus. Like our previous study on the rat brain and human neocortex, immunoreactivity for A2 and B1 was observed mainly in the nucleoplasm in neurons [9,10,15]. In the present study, we observed intense A2 and B1 immunoreactivity, although some variations in immunoreactivity were observed depending on the hippocampal regions. Since the intensity of immunoreactivity for these proteins may, in part, reflect post-transcriptional regulations, it is possible that in the human hippocampus, A2- and B1-associated post-transcription is highly activated, and post-trascriptional regulations associated with A2 and B1 are different from region to region.

In the AD hippocampus, we observed different alterations between A2 and B1. In the subjects with severe AD pathology, A2 immunoreactivity was increased in neurons within the CA fields except for CA1, while B1 immunoreactivity was decreased throughout the hippocampus. Interestingly, in our previous study, we observed increased A2 immunoreactivity and decreased B1 immunoreactivity in the hippocampal neurons 1, 3, 7, and 14 days after deafferentation of the perforant pathway on the rat brain [9]. The perforant pathway is well known as one of the most severely affected regions in the AD brain [8]. Thus, it is possible to suppose that alterations in A2 and B1 immunoreactivity observed in the AD hippocampus in the present study are in response to the deafferentation of the perforant pathway in the AD brain. Since A2 and B1 are produced by alternative splicing from a single copy gene [12], it is also possible that in response to AD pathology, neurons shift production from B1 to A2. It is documented that A2 has a function of mRNA trafficking in the neuronal dendrites as well as post-transcriptional regulation [20]. In line with this functional property of A2, we observed A2 immunoreactivity in the neuronal cytoplasm and proximal dendrites as well as in the nucleoplasm. In vitro study demonstrated that A2 binds many mRNAs localized in the dendrites, such as MAP2A, Arc, and GABA receptor α subunit [16]. In addition, neurons from CA4 to CA2 (i.e., the resistant zone) increased A2 but not in the CA1 subfield (i.e., the vulnerable zone). When these findings are taken together, it is plausible to suppose that neurons increase A2 to compensate for the dendritic damage in AD pathology.

In our previous study [10], we reported relative preservation of B1 immunoreactivity in the inferior temporal cortex of the AD brain. These observations appear inconsistent with the findings in the present study, that B1 immunolabeling decreased in the CA1 subregion in the moderately affected subjects, and in the severely affected cases, a decrease in B1 was observed in more extensive regions. One possible explanation for these inconsistent data is due to a difference of pathological severity between the hippocampus and the inferior temporal cortex. It is well known that AD pathology is much more severe in the hippocampus than in the neocortices. Thus, it is plausible to conclude that a decrease in B1 occurs in the advanced AD pathology.

We observed a decrease in A2 and B1 immunoreactivity in tangle-bearing neurons. Previous study demonstrated that total cellular RNA and polyadenylated RNA were substantially reduced in the AD cortex with neurofibrillary tangles [19]. In addition, the study of Ginsberg et al. [6] showed that tangle-bearing neurons reduced several classes of mRNAs that are known to encode proteins implicated in AD neuropathology. Although it remains to be determined whether post-transcriptional processes of these proteins are regulated by A2/B1, our study with double immunohistochemistry suggests that A2- and B1-associated post-transcriptional regulations are disturbed in NFT-bearing neurons.

Our study suggests that hnRNP A2 and B1 display a different response to AD pathology, with A2 being more resistant to AD pathology. The findings of increased A2 immunoreactivity in survival neurons in the resistant zone raise the possibility that neurons increase A2 in some compensatory mechanisms as a part of AD pathology. The double immunohistochemical studies suggest that A2- and B1-associated post-transcriptional regulations are disturbed in NFT- bearing neurons of the AD brain.

Acknowledgement

This work was supported by the Research Grant for Longevity Sciences (14C-4) from the Ministry of Health, Labour and Welfare.

References

[1] S. Akbarian, M.A. Smith, E.G. Jones, Editing for an AMPA receptor subunit RNA in prefrontal cortex and striatum in Alzheimer's disease, Huntington's disease and schizophrenia, Brain Res. 699 (1995) 297–304.
[2] American Psychiatric Association, Diagnostic and Statistical Manual of Mental Disorders, fourth ed., American Psychiatric Association, Washington, DC, 1994.
[3] H. Braak, E. Braak, Neuropathological staging of Alzheimer-related changes, Acta Neuropathol. (Berl.) 82 (1991) 239–259.
[4] G. Dreyfuss, M.J. Matunis, S. Piñol-Roma, C.G. Burd, HnRNP proteins and the biogenesis of mRNA, Annu. Rev. Biochem. 62 (1993) 289–321.
[5] H.M. Duvernoy, The Human Hippocampus, second ed, Springer-Verlag, Berlin, 1998.
[6] S.D. Ginsberg, S.E. Hemby, V.M. Lee, J.H. Eberwine, J.Q. Trojanowski, Expression profile of transcripts in Alzheimer's disease tangle-bearing CA1 neurons, Ann. Neurol. 48 (2000) 77–87.
[7] K. Honda, M.A. Smith, X. Zhu, D. Baus, W.C. Merrick, A.M. Tartakoff, T. Hattier, P.L. Harris, S.L. Siedlak, H. Fujioka, Q. Liu, P.I. Moreira, F.P. Miller, A. Nunomura, S. Shimohama, G. Perry, Ribosomal RNA in Alzheimer disease is oxidized by bound redox-active iron, J. Biol. Chem., March 14 (2005) (Epub. ahead of print).
[8] B.T. Hyman, G.W. Van Hoesen, A.R. Damasio, Alzheimer's disease: glutamate depletion in the hippocampal perforant pathway zone, Ann. Neurol. 22 (1987) 37–40.
[9] M. Ishikawa, K. Mizukami, M. Iwakiri, S. Hidaka, H. Kamma, T. Asada, Alterations of the hnRNP A2 and B1 in the hippocampus of the rat after perforant pathway lesion, Acta Neuropathol. (Berl.) 107 (2004) 144–148.
[10] M. Ishikawa, K. Mizukami, M. Iwakiri, H. Kamma, M.D. Ikonomovic, S.T. Dekosky, T. Asada, Immunohistochemical study of hnRNP B1 in the postmortem temporal cortices of patients with Alzheimer's disease, Neurosci. Res. 50 (2004) 481–484.
[11] H. Kamma, H. Satoh, M. Matsui, W.W. Wu, M. Fujiwara, H. Horiguchi, Characterization of hnRNP A2 and B1 using monoclonal antibodies: intracellular distribution and metabolism through cell cycle, Immunol. Lett. 76 (2001) 49–54.
[12] T. Kozu, B. Henrich, K.P. Schafer, Structure and expression of the gene (HNRPA2B1) encoding the human hnRNP protein A2/B1, Genomics 25 (1995) 365–371.
[13] S. Li, M. Mallory, M. Alford, S. Tanaka, E. Masliah, Glutamate transporter alterations in Alzheimer disease are possibly associated with abnormal APP expression, J. Neuropathol. Exp. Neurol. 56 (1997) 901–911.
[14] G. McKhann, D. Drachman, M. Folstein, R. Katzman, D. Price, E.M. Stadlan, Clinical diagnosis of Alzheimer's disease: report of the NINCDS-ADRDA Work Group under the auspices of Department of Health and Human Services Task Force on Alzheimer's Disease, Neurology 34 (1984) 939–944.
[15] K. Mizukami, H. Kamma, M. Ishikawa, G. Dreyfuss, Immunohistochemical study of the hnRNP A2 and B1 in the rat forebrain, NeuroReport 11 (2000) 3099–3102.
[16] T.P. Munro, R.J. Magee, G.J. Kidd, J.H. Carson, L. Bararese, L.M. Smith, R. Smith, Mutational analysis of a heterogeneous nuclear ribonucleoprotein A2 response element for RNA trafficking, J. Biol. Chem. 274 (1999) 34389–34395.
[17] L. Otvos Jr., L. Feiner, E. Lang, G.I. Szendrei, M. Goedert, V.M. Lee, Monoclonal antibody PHF-1 recognizes tau protein phosphorylated at serine residues 396 and 404, J. Neurosci. Res. 39 (1994) 669–673.
[18] S. Piñol Roma, G. Dreyfuss, Shuttling of premature mRNA bindings proteins between nucleus and cytoplasm, Nature 355 (1992) 730–732.
[19] E.M. Sajdel-Sulkowska, C.A. Marotta, Alzheimer's disease brain: alterations in RNA levels and in a ribonuclease-inhibitor complex, Science 225 (1984) 947–949.
[20] J. Shan, T.P. Munro, E. Barbarese, J.H. Carson, R. Smith, A molecular mechanism for mRNA trafficking in neuronal dendrites, J. Neurosci. 23 (2003) 8859–8866.
[21] W. Wallace, S.T. Ahlers, J. Gotlib, V. Bragin, J. Sugar, R. Gluck, P.A. Shea, K.L. Davis, V. Haroutunian, Amyloid precursor protein in the cerebral cortex is rapidly and persistently induced by loss of subcortical innervation, Proc. Natl. Acad. Sci. U.S.A. 90 (1993) 8712–8716.
[22] W.C. Wallace, V. Bragin, N.K. Robakis, K. Sambamurti, D. VanderPutten, C.R. Merril, K.L. Davis, A.C. Santucci, V. Haroutunian, Increased biosynthesis of Alzheimer amyloid precursor protein in the cerebral cortex of rats with lesions of the nucleus basalis of Meynert, Mol. Brain Res. 10 (1991) 173–178.

ELSEVIER

NeuroImage

www.elsevier.com/locate/ynimg
NeuroImage 28 (2005) 1014 – 1021

The prediction of rapid conversion to Alzheimer's disease in mild cognitive impairment using regional cerebral blood flow SPECT

Kentaro Hirao,[a,c] Takashi Ohnishi,[a,b,*] Yoko Hirata,[a] Fumio Yamashita,[a] Takeyuki Mori,[a] Yoshiya Moriguchi,[a] Hiroshi Matsuda,[a,f] Kiyotaka Nemoto,[a,d] Etsuko Imabayashi,[a,f] Minoru Yamada,[a,f] Toshihiko Iwamoto,[c] Kunimasa Arima,[c] and Takashi Asada[d]

[a]*Department of Radiology, National Center Hospital of Mental, Nervous, and Muscular Disorders, National Center of Neurology and Psychiatry, Tokyo, Japan*
[b]*Department of Investigative Radiology, Research Institute, National Cardiovascular Center, Osaka, Japan*
[c]*Department of Laboratory Medicine, National Center Hospital of Mental, Nervous, and Muscular Disorders, National Center of Neurology and Psychiatry, Tokyo, Japan*
[d]*Department of Psychiatry, Institute of Clinical Medicine, University of Tsukuba, Japan*
[e]*Department of Geriatric Medicine, Tokyo Medical University, Japan*
[f]*Department of Nuclear Medicine, Saitama Medical School, Japan*

Received 13 April 2005; revised 7 June 2005; accepted 30 June 2005
Available online 29 August 2005

Mild cognitive impairment (MCI) comprises a heterogeneous group with a variety of clinical outcomes and they are at risk for developing Alzheimer's disease (AD). The prediction of conversion from MCI to AD using the initial neuroimaging studies is an important research topic. We investigated the initial regional cerebral blood flow (rCBF) measurements using single photon emission computed tomography (SPECT) in individuals with 76 amnesic MCI (52 subjects converted to AD and 24 subjects did not convert to AD at 3-year follow-up) and 57 age- and gender-matched controls. We sought functional profiles associated with conversion to AD, then evaluated the predictive value of the initial rCBF SPECT. As compared with controls, AD converters demonstrated reduced blood flow in the bilateral parahippocampal gyri, precunei, posterior cingulate cortices, bilateral parietal association areas, and the right middle temporal gyrus. Non-converters also demonstrated significant reduction of rCBF in the posterior cingulated cortices and the right caudate nucleus when compared to controls. As compared with non-converters, converters showed reductions of rCBF in the bilateral temporo-parietal areas and the precunei. The logistic regression model revealed that reduced rCBF in the inferior parietal lobule, angular gyrus, and precunei has high predictive value and discriminative ability. Although a cross-validation study is needed to conclude the usefulness of rCBF SPECT for the prediction of AD conversion in individuals with MCI, our data suggest that the initial rCBF SPECT studies of individuals with MCI may be useful in predicting who will convert to AD in the near future.

Keywords: Mild cognitive impairment (MCI); Alzheimer's disease (AD); Regional cerebral blood flow (rCBF); Single photon emission computed tomography (SPECT)

Introduction

Mild cognitive impairment (MCI) is an operational diagnostic term developed to describe the preclinical stage of Alzheimer's disease (AD) (Petersen et al., 2001a). The risk for conversion to AD is higher in individuals with MCI than in the general aged population, as annual conversion rate of 6%–25% from MCI to AD (Petersen et al., 2001b). Furthermore, a recent study suggested that progression from MCI to AD is time-dependent. According to Palmer's study, people with MCI have a high risk of progressing to dementia over the next 3 years, and the risk starts to decrease after this point (Palmer et al., 2003). The early detection of MCI individuals who will later convert to AD is an important issue for both clinical and research interests.

The recent advance of computer-assisted statistical image analyses revealed that subjects with very mild AD typically show abnormal metabolic and regional cerebral blood flow (rCBF) patterns, even at the preclinical stage. Using glucose metabolism positron emission tomography (PET) with a voxel-by-voxel statistical analysis, Minoshima et al. reported that the earliest changes observed in very mild AD were in the posterior cingulate cortex (PCC) (Minoshima et al., 1997). This unexpected finding has

* Corresponding author. Department of Radiology, National Center Hospital of Mental, Nervous, and Muscular Disorders, National Center of Neurology and Psychiatry 4-1-1 Ogawa Higashi, Kodaira City, Tokyo 187-0031, Japan.
E-mail address: tohnishi@hotmail.com (T. Ohnishi).
Available online on ScienceDirect (www.sciencedirect.com).

1053-8119/$ - see front matter © 2005 Elsevier Inc. All rights reserved.
doi:10.1016/j.neuroimage.2005.06.066

been replicated by other groups using both glucose metabolism measurements with PET and even less sophisticated measurement techniques such as regional cerebral blood flow (rCBF) measurements with single photon emission computed tomography (rCBF SPECT). Our previous rCBF SPECT study demonstrated significantly decreased rCBF in the posterior cingulate gyri and precunei bilaterally in MCI subjects as compared with controls at least 2 years before they met a clinical diagnosis of AD (Kogure et al., 2000). We also reported a diagnostic value of reduced rCBF in the posterior cingulate cortex (PCC) to assist in discriminating between normal subjects and MCI subjects who later developed AD (Imabayashi et al., 2004). Furthermore, a PET study demonstrated hypometabolism of the PCC in young subjects with a high genetic risk of developing AD (Reiman et al., 2004). These results suggest that functional neuroimaging techniques such as PET and SPECT may be promising techniques for the preclinical diagnosis of AD.

However, MCI is a heterogeneous diagnostic category comprised of individuals with a variety of clinical outcomes (Petersen et al., 2001). As such, only a longitudinal study comparing MCI subjects who convert to AD at follow-up (converters) with MCI subjects who do not convert at follow-up (non-converters) is appropriate to determine the predictive value of initial neuroimaging for progression of MCI to AD. Only a few longitudinal studies have been published so far (Celsis et al., 1997; Arnaiz et al., 2001; Huang et al., 2002; Chetelat et al., 2003; Drzezga et al., 2003; Mosconi et al., 2004). These studies have suggested that reduced glucose metabolism in the right temporo-parietal cortex or reduced rCBF and glucose metabolism in the PCC might be good predictors of progression to AD.

On the other hand, morphological magnetic resonance imaging (MRI) studies have demonstrated that higher atrophy rates in the medial temporal regions such as the entorhinal cortex and hippocampus may be good predictors of conversion to AD (Jack et al., 1999; Mungas et al., 2002; Nestor et al., 2004). However, such serial MR studies require at least a 1-year follow-up period to predict AD conversion. As with functional imaging studies, the predictive value of morphological MR studies has not been yet clarified.

The present retrospective cohort study assessed initial rCBF SPECT images in a group of amnesic MCI subjects consisting of AD converters and non-converters who were followed clinically for 3 years. The aim of the present study was to find highly specific and sensitive rCBF changes capable of discriminating between MCI subjects who eventually develop AD from those who do not convert to AD, as early as possible. We also demonstrated the predictive value of the initial rCBF SPECT studies in MCI subjects.

Methods

Subjects

The characteristics of the subjects who participated in this study are summarized in Table 1. We retrospectively studied 82 individuals (40 men and 42 women) with MCI who visited our memory clinic with a chief complaint of memory disturbance. Six MCI subjects (3 men and 3 women) dropped out and therefore their outcomes were unknown. Analyses therefore included 76 MCI subjects (37 men and 39 women) and 57 age- and gender-matched control subjects. All subjects were free of depression as operationalized as a score less than 8 on the Hamilton Depression Scale (Hamilton, 1960). MCI was diagnosed using the criteria proposed by Mayo Clinic Alzheimer's Disease Research Center. Recently, the criteria of MCI was modified (Pertersen, 2004), but when our study was conducted, the criteria required: (1) memory complaint by patient, family, or physician; (2) normal activities of daily living; (3) normal global cognitive function; (4) objective impairment in memory or in one other area of cognitive function as evident by scores >1.5 SD below the age appropriate mean; (5) CDR score (Hughes et al., 1982) of 0.5; and (6) absence of dementia.

MCI subjects ranged in age from 48 to 86 years with a mean ± standard deviation (SD) of 69.0 ± 8.6 years. The Mini-Mental State Examination (MMSE) (Folstein et al., 1975) score ranged from 24 to 29 (mean ± SD 26.5 ± 1.6) at the initial visit. During the subsequent follow-up period of 3 years, 52 patients showed progressive cognitive decline and eventually fulfilled the diagnosis

Table 1
The characteristics of subjects

	MCI (M:F = 37:39)			Results of ANOVA	
	Controls (M:F = 30:27)	Non-converters (M:F = 12:12)	Converters (M:F = 25:27)	*F* value	*P* value
Age	70.4 ± 7.3	68.7 ± 7.6	69.2 ± 9.1	0.5	0.6
Education in years	12.2 ± 2.9	12.2 ± 3.1	12.0 ± 3.1	0.1	0.9
MMSE	28.8 ± 1.5	27.0 ± 1.3*	26.2 ± 1.7*	38.7	<0.001
MMSE (about after 3 years)		26.1 ± 1.4*	19.1 ± 4.3*********	126.1	<0.001
Digit span					
Forward	5.3 ± 1.0	5.6 ± 1.0	5.4 ± 1.0	0.5	0.6
Backward	4.1 ± 0.8	4.2 ± 0.8	4.1 ± 1.0	0.2	0.8
List learning (10 words)					
Delayed recall (30 min)	7.9 ± 1.2	3.7 ± 3.6*	0.9 ± 2.0*******	117	<0.001
Story recall (15 elements)					
Delayed (30 min)	7.9 ± 2.5	0.87 ± 1.72*	0.9 ± 1.72*	101.8	<0.001
Rey–Osterrieth complex figure test					
Delayed recall (30 min)	14.47 ± 6.31	4.28 ± 3.76*	2.9 ± 6.93***	85.3	<0.001

Note. Data are mean ± SD in controls (n = 57) or MCI (n = 76).

* Scores of MCI are significantly lower than those of controls, $P < 0.05$ (Bonferroni correction for multiple comparison).

** Scores of the converters are significantly lower than those of non-converters, $P < 0.05$ (Bonferroni correction for multiple comparison).

*** Scores of the converters are significantly lower than those of non-converters, $P < 0.001$ (Bonferroni correction for multiple independent comparisons).

**** Scores of the follow up MMSE are significantly lower than those of the initial MMSE, $P < 0.05$ (paired t test).

of probable AD according to the National Institute of Neurologic and Communicative Disorders and Stroke and the Alzheimer's Disease and Related Disorders Association criteria (NINCDS-ADRDA) (McKhann et al., 1984). Twenty-four of the 76 MCI subjects still did not fulfill the criteria for dementia according to DSM-IV (American Psychiatric Association, 1994) during the follow-up period. Of these participants, 40 converters and 12 non-converters completed follow-up rCBF SPECT studies at the end of the 3-year follow-up period.

Fifty-seven individuals (30 men and 27 women; age 56–86 years, mean ± SD 70.4 ± 7.3 years) did not have memory impairment or cognitive disorders and were assigned to the normal control group. Specifically, their performances were within normal limits (<1 SD) both on the Wechsler Memory Scale-Revised and on the Wechsler Adult Intelligence Scale-Revised, and their MMSE score ranged from 25 to 30 (mean ± SD 28.8 ± 1.5). None of these control subjects manifested cognitive changes during the follow-up period of more than 3 years. The control group did not differ significantly in age or education from the MCI group.

The local ethics committee approved this study for both healthy volunteers and MCI subjects, all of whom gave their informed consent to participate. All subjects were right-handed and screened by questionnaire regarding medical history and excluded if they had neurological, psychiatric, or medical conditions that could potentially affect the central nervous system, such as substance abuse or dependence, atypical headache, head trauma with loss of consciousness, asymptomatic or symptomatic cerebral infarction detected by T2-weighted MRI, hypertension, chronic lung disease, kidney disease, chronic hepatic disease, cancer, or diabetes mellitus.

SPECT imaging

Before the SPECT scan was performed, all subjects had an intravenous line established. They were injected while lying supine with eyes closed in a dimly lit quiet room. Each subject received an intravenous injection of 600 MBq of technetium-99 m ethyl cysteinate dimer (99 mTc-ECD). Ten minutes after the injection of 99 mTc-ECD, brain SPECT was performed using three-head rotating gamma cameras (Multispect3; Siemens Medical Systems, Inc., Hoffman Estates, IL) equipped with high-resolution fan-beam collimators. For each camera, projection data were obtained in a 128 × 128 format for 24 angles at 50 s per angle. A Shepp and Logan Hanning filter was used for SPECT image reconstruction at 0.7 cycle/cm. Attenuation correction was performed using Chang's method.

Statistical parametric mapping

Images were analyzed with the statistical parametric mapping software SPM99 (Wellcome Department of Cognitive Neurology, UK). Using a template for Tc-99 m ECD template, the SPECT data were transformed into a standard stereotaxic space (MNI). The spatial normalization algorithm of SPM99 was used for linear and non-linear transformation (basis function: 8 × 9 × 8: iteration: 16). A Gaussian filter (12 mm full width at half maximum) was used to smooth each image. The effect of global differences in CBF between scans was removed by proportional scaling with the threshold at 60% of whole brain activity. Using MRIcro (www.mricro.com), we checked the mask image for statistical analysis and verified that medial temporal regions including the parahippocampal gyrus and hippocampus were encompassed in the analysis. To test hypotheses about regional population effects, data were analyzed by analysis of variance (ANOVA) using the full monthly option. For this F test, we used an alpha value of 0.001 as our level of significance to correct for multiple comparisons. Group comparisons were also done using t tests within the ANOVA design matrix (uncorrected $P < 0.001$ and cluster extent $K > 100$ voxels, small volume correction (SVC) for correction of multiple comparisons). There were twice as many converters as non-converters raising the concern that the SPECT abnormalities in the former might be influenced by statistical power. Therefore, we randomly subdivided AD converters into 2 groups where the group size was matched to that of non-converters. Then, two-sample t tests between non-converters and each group of AD converters were done (uncorrected $P < 0.001$). The resulting sets of t values constituted the statistical parametric maps {SPM (t)}. Anatomic localization was identified using both MNI coordinates and Talairach coordinates obtained from M. Brett's transformations (http://www.mrc-cbu.cam.ac.uk/Imaging/mnispace.html) and were presented as Talairach coordinates (Talairach and Tournoux, 1988).

Logistic regression model

To evaluate the predictive value of rCBF change observed in the initial rCBF SPECT, we used as independent variables (X1) Z scores for the mean adjusted rCBF value at the significant clusters obtained from the SPM (t) map in the group comparison (AD converter vs. Non-converter) for the logistic regression model:

$$Y = b0 + b1*X1$$

where Y is the logit transformation of the probability P. The logit transformation of the probability of a value is defined as:

$$Y = \log(P/(1 - P))$$

where P is the probability of conversion from MCI to AD.

The mean value of the adjusted rCBF in each cluster of each subject was extracted using the Marsbar program (http// www.marsbar.sourceforge.net/), then the Z score was calculated using the following formula: Z score = (mean adjusted rCBF value in the control group minus individual value of adjusted rCBF value)/SD of rCBF value in the control group. The logistic regression model analysis was performed using Statistical Package for the Social Sciences (SPSS, Japan Co., Tokyo, Japan). Because the neuropsychological test scores of converters were significantly lower than those of non-converters (especially on delayed recall of list learning and delayed recall of Rey–Osterrieth Complex Figure Test), we also evaluated the predictive value of those scores at the initial visit using logistic regression analysis.

Results

Conversion rate

In our study, 52 of 82 individuals with MCI converted to AD during the 3-year follow-up period. The annual conversion rate of MCI to AD was approximately 21.14%.

Group comparisons

The ANOVA analysis [SPM (F), $P < 0.001$, corrected for multiple comparisons with family-wise alpha < 0.05] revealed a significant difference among groups in the bilateral precunei (Brodmann area [BA] 7), the posterior cingulate cortices (PCC, BA31, peak $x, y, z = 0, -47, 32$, F value = 35.93), the right inferior parietal lobule (BA40, peak $x, y, z = 46, -64, 44$, F value = 25.23) and the left angular gyrus (BA39, peak $x, y, z = -42, -60, 38$, F value = 16.77) (Fig. 1a). In comparison with controls, AD converters demonstrated reduced blood flow in the bilateral parahippocampal gyri, precunei, PCC, bilateral parietal association areas, and the right middle temporal gyrus (Fig. 1b, Table 2). Non-converters also demonstrated significant reduction of rCBF in the PCC and the right caudate nucleus when compared to controls (Fig. 1c, Table 2). Importantly, significant differences in the bilateral precunei and parietal association areas were found between converters and non-converters (Fig. 1d, Table 2).

Group comparisons of subdivided groups of converters and the non-converters

As compared to non-converters, the first group of 26 converters showed significantly decreased rCBF in the right inferior parietal lobule (Talairach coordinate: 46, −64, 47, t value: 3.82, cluster size: 115) and the left angular gyrus (Talairach coordinate: −40, −58, 36, t value: 4.45, cluster size: 127) (Fig. 2 left). The essentially same result was found in the comparison between non-converters and the second group of 26 converters (Right IPL: Talairach coordinate: 53, −58, 42, t value: 3.65, cluster size: 44; Left angular gyrus: Talairach coordinate: −40, −57, 34, t value: 4.81, cluster size: 180) (Fig. 2, right). We could not find reduced rCBF in the precunei at $P < 0.001$; however, reduction in the precunei was detected at a lenient statistical threshold ($P < 0.005$ without multiple comparisons) in each group comparison (data were not shown).

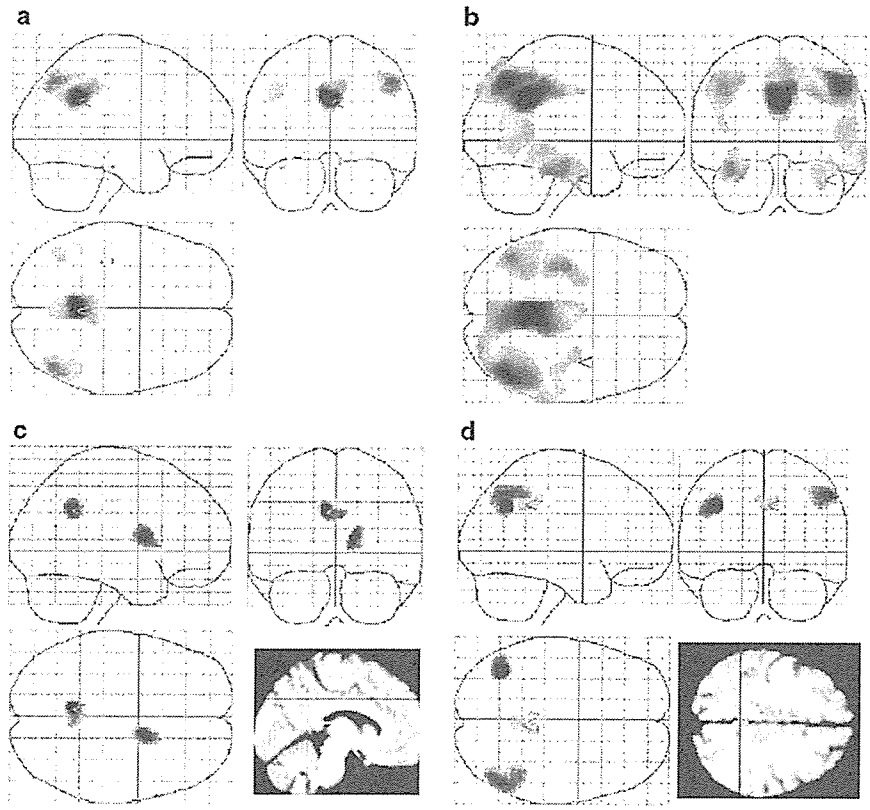

Fig. 1. Results of group comparisons. (a) The SPM {F} is displayed in a standard format as a maximum-intensity projection viewed from the right, the back, and the top of the brain. The anatomical space corresponds to the atlas of Talairach and Tournoux. Representation in stereotaxic space of regions with significantly differences between groups (corrected $P < 0.05$) was demonstrated. The ANOVA demonstrated a significant difference among groups in the bilateral precunei, the posterior cingulate cortices, the right inferior parietal lobule, and the left angular gyrus. (b) The SPM is displayed in a standard format as a maximum-intensity projection of regions with significantly decreased rCBF in converters compared with the control group [$P < 0.001$, corrected by small volume correction (SVC)]. The converters demonstrated reduced blood flow in the bilateral parahippocampal gyri, precunei, PCC, bilateral parietal association areas, and the right middle temporal gyrus. (c) The SPM is displayed in a standard format as a maximum-intensity projection of regions with significantly decreased rCBF in non-converters compared with the control group ($P < 0.001$, corrected by SVC). Non-converters demonstrated significant reduction of rCBF in the PCC and the right caudate nucleus. (d) The SPM is displayed in a standard format as a maximum-intensity projection of regions with significantly decreased rCBF in converters compared with non-converters ($P < 0.001$, corrected by SVC). The converters showed a significant reduction of rCBF in the bilateral precunei and parietal association areas.

Table 2
Results of group comparisons and paired t tests

Region	BA	Coordinates			K	Corrected P value (with small volume correction)	t value
		x	y	z			
Controls > AD converters							
Bilateral precuneus, and PCC	BA31						
	B7	2	−45	32	6794	<0.001	8.46
R IPL	BA40	46	−64	44	6794	<0.001	6.95
L Angular gyrus, IPL	BA39	−42	−60	38	1301	<0.001	5.24
L PHG	BA20,36	−38	−22	−17	771	<0.001	5.36
R PHG	BA20,36	34	−15	−19	535	0.005	3.97
R Middle temporal gyrus	BA21	63	−37	−8	535	0.008	4.25
Controls > MCI non-converters							
L PCC	BA31	−8	−49	34	231	<0.001	4.83
R PCC	BA31	4	−47	30	231	0.003	3.81
R Caudate nucleus		14	6	11	158	<0.001	4.63
MCI non-converters > AD converters							
R IPL	BA40	51	−58	45	653	0.001	4.49
L Angular gyrus	BA39	−38	−58	36	368	<0.001	5.21
L Precuneus	BA7	−6	−35	42	140	0.014	3.34
R Precuneus	BA7	2	−45	43	140	0.009	3.51

BA: Brodmann area, IPL: inferior parietal lobule, PCC: posterior cingulate cortex, PHG: Parahippocampal gyrus.

The predictive value of rCBF changes observed at initial SPECT and scores of neuropsychological tests

Given the results of the group comparisons, we hypothesized that rCBF changes in the precuneus and the parietal association areas would be good predictors of progression from MCI to AD in individuals with MCI. Using the Z score of each region (Fig. 3) for each MCI subject, we determined the predictive value of the initial rCBF SPECT using a logistic regression analysis. Table 3 shows the results of the logistic regression analysis. We found that higher Z scores in the left angular area (Wald $\chi^2 = 11.1$, $df = 1$, $P = 0.001$, odds ratio [OR] 2.174, 95% confidence interval [CI] = 1.38–3.43), right inferior parietal lobule (Wald $\chi^2 = 10.7$, $df = 1$, $P = 0.001$, OR 2.13, 95% CI = 1.35–3.35), and the precuneus (Wald $\chi^2 = 10.13$, $df = 1$, $P = 0.001$, OR 2.417, 95% CI = 1.4–4.16) were good predictors of progression from MCI to AD (Table 3). A cutoff value of 0.5, which best divided the converter and non-converters, provided high sensitivity (82–90%) and adequate overall accuracy (68–73%) in each region (Table 3).

In contrast, lower scores on delayed recall of list learning (Wald $\chi^2 = 8.369$, $df = 1$, $P = 0.004$, odds ratio [OR] 1.413, 95% confidence interval [CI] = 1.118–1.786) and lower scores on delayed recall of the Rey–Osterrieth Complex Figure Test (ROCFT) (Wald $\chi^2 = 7.092$, $df = 1$, $P = 0.008$, OR 1.167, 95% CI = 1.042–1.308) had lower predictive values than those of the rCBF changes observed in SPECT studies. A cutoff value of 0.5, which best divided the converters and non-converters, revealed similar sensitivity (90.3% for word leaning and 86.2% for ROCFT,

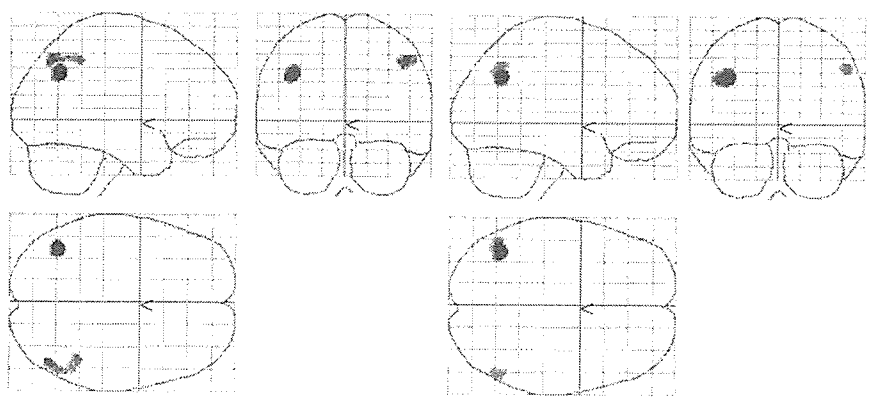

Fig. 2. Results of group comparisons of subdivided groups of converters and the non-converters. The SPM is displayed in a standard format as MIP of regions with significantly decreased in rCBF in converters compared with non-converters (uncorrected $P < 0.001$). Fifty-two converters were randomly divided two groups. Then, two-sample t tests between non-converters and each group of AD converters were done. Left: The first group of converters showed a significantly decreased rCBF in the left angular gyrus and the right inferior parietal lobule. Right: The second group of converters also showed essentially the same result.

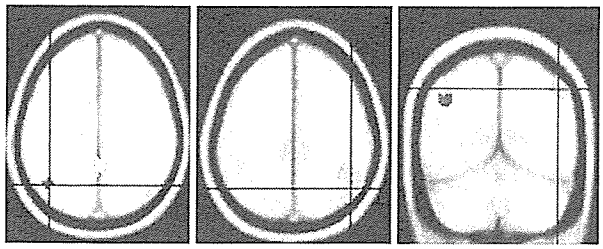

Fig. 3. Regions of interest (ROIs) for the logistic regression model. Red: The ROI for the *Z* score in the left angular gyrus. Yellow: The ROI for the *Z* score in the bilateral precunei. Green: The ROI for the *Z* score in the right inferior parietal lobule.

respectively) and overall accuracy (69.8% for word leaning and 78% for ROCFT respectively) to the sensitivity and accuracy associated with the rCBF changes observed in the initial SPECT (Table 3).

Discussion

The conversion rate

The annual conversion rate of MCI to AD in the current study was 21.14%, which is higher than that observed in other cohorts of MCI subjects (Bruscoli and Lovestone, 2004). A recent review of conversion studies reported that the overall rate of conversion was 10%, but that large differences existed between studies (Bruscoli and Lovestone, 2004). The single most important variable accounting for between-study heterogeneity was the source of subjects, with self-selected clinic attendees having the highest conversion rate (Bruscoli and Lovestone, 2004). In our study, all individuals with MCI were outpatients that attended a memory clinic, and therefore the high conversion rate in the study is not surprising.

Different rCBF changes between converters and non-converters and the predictive value of initial SPECT study

In this study, converters displayed a significant reduction of rCBF in the precuneus and bilateral parietal association areas when compared to non-converters. Although the sample size of converters was larger than that of non-converters, the results of group comparisons with randomly re-sampling the converters in cohorts where the sample sizes were matched to that of non-converters demonstrated essentially the same results. The fact indicated that the greater extent of rCBF abnormalities in converters was not influenced by statistical power. Importantly, we also found that reduction of rCBF in these areas is a good predictor of conversion from MCI to AD. Performance on measures of delayed recall of word learning and ROCFT also showed relatively high discriminative ability, although these scores had lower odds ratios than those associated with reduction of rCBF. These results demonstrate the utility of rCBF SPECT for the prediction of AD conversion. Previous functional neuroimaging studies in very early AD and MCI have consistently demonstrated dysfunction in the PCC and cinguloparietal transitional area or precuneus (Minoshima et al., 1997; Kogure et al., 2000; Imabayashi et al., 2004). A recent PET study showed that the retrosplenial PCC was the only abnormality common to all MCI individuals (Nestor et al., 2003a,b). However, our data suggest that reduced rCBF in the parietal association areas and precuneus are better predictors than PCC hypoperfusion. Indeed, the comparison between the controls and non-converters also demonstrated a significant reduction of rCBF in the PCC. We consider that hypoperfusion in the temporo-parietal regions could be more advanced signs of AD pathology and may precede manifestation of clinical symptoms of AD, and therefore they were better predictors of early conversion. A recent longitudinal FDG-PET study reported similar results to those of the present study: a high predictive value of reduced FDG uptake in the parietal association areas and a lower predictive value of that in the PCC (Chetelat et al., 2003). Mosconi et al. also reported that converters demonstrated reduced glucose metabolism in the inferior parietal cortex as compared with non-converters (Mosconi et al., 2004). Although Nestor's study emphasized the importance of functional abnormality of the retrosplenial cortex in MCI subjects, they also reported that MCI subjects with additional hypometabolism in the parietal association areas converted to AD during the follow-up period (Nestor et al., 2003). These results in conjunction with the current results strongly demonstrate the high predictive value of functional abnormality in the parietal association areas. Furthermore, these results are consistent with the results of a postmortem study of tau pathology in aging and AD (Delacourte et al., 1999). According to Delacourte's study, neurofibrillary degeneration (NFD) with paired helical filaments (PHF)-tau was systematically present in varying amounts in the hippocampal region of non-demented aged subjects, whereas tau pathology in the angular gyrus (BA39) and dorsolateral prefrontal cortex (BA9) was found in all AD patients

Table 3
Results of logistic regression model

	Odds ratio	95% CI	*P* value	Sensitivity (%)	Overall accuracy (%)
SPECT imaging test					
Regions					
L Angular gyrus	2.174	1.38–3.43	<0.001	82	68
R IPL	2.130	1.35–3.35	<0.001	90	73.3
Precuneus	2.417	1.40–4.161	<0.001	88	73.3
Neuropsychological test					
List learning (delayed recall)	1.413	1.118–1.786	0.004	90.3	69.8
Rey–Osterrieth complex figure test (delayed recall)	1.167	1.042–1.308	0.008	86.2	78

CI: confidence interval, IPL: inferior parietal lobule.

(Delacourte et al., 1999). The data support the notion that functional abnormality in the parietal association areas should be a *better predictor* of AD conversion. However, two longitudinal studies (Huang et al., 2002; Drzezga et al., 2003) suggested high predictive value of functional abnormality in the PCC; further study will be needed to clarify the predictive value of the functional abnormality in the PCC.

Unexpectedly, we found decreased rCBF in the right caudate nucleus in comparing controls and non-converters. A recent voxel-based volumetric MR study (Frisoni et al., 2002) revealed reduced gray matter volume of caudate nucleus in mild AD; however, we have no good explanation or hypothesis about this finding at the present moment.

Reduction of rCBF in the parahippocampal gyrus in converters

In this study, we found reduced parahippocampal rCBF in converters. Numerous structural MRI studies have demonstrated that progressive atrophy of the parahippocampal area including the entorhinal cortex is a sensitive marker for detecting and predicting AD (Chetelat and Baron, 2003; Korf et al., 2004; Nestor et al., 2004). In this study, we did not apply a partial volume effect (PVE) correction for SPECT imaging; therefore, one could argue that reduced rCBF in the parahippocampal area could be explained by partial volume effect. We agree that PVE partially contributes to the results of our study. However, an atrophy-corrected FDG-PET study demonstrated hippocampal hypometabolism in AD and MCI and the study's authors concluded that metabolism reductions exceed volume losses in MCI (De Santi et al., 2001). Other studies with MRI-guided FDG-PET also demonstrated hypometabolism of the limbic systems (de Leon et al., 2001; Nestor et al., 2003a,b) including the entorhinal cortex in MCI.

Limitations of this study

The first limitation of this study is that we did not evaluate the cross-validity of the predictive value of the SPECT findings using split-half reliability due to the limited number of non-converters. To conclude the usefulness of rCBF SPECT in predicting AD conversion, our data should be replicated in other cohorts. In this context, our data may be considered to be preliminary rather than conclusive. However, other studies conducted by different research groups using a different imaging method (FDG-PET) reported similar results to those of the present study (Chetelat et al., 2003), and we believe that our predictive model should be reliable.

Second, we did not perform the correction of partial volume effects (PVE) for SPECT images. We agree that PVE could partially contribute to the results of the present study. Even so, the predictive value of rCBF patterns identified in this study still has diagnostic value. From a diagnostic point of view, atrophy-related hypoperfusion is a consequence of AD pathology and might improve the detection of early functional abnormalities.

Finally, some may argue that a 3-year follow-up is not long enough. We agree that it remains a possibility that some of the non-converters would develop AD during a longer observation period, because the logistic model cannot be certain that someone will not convert AD after the follow-up period. However, we can still distinguish rapid converters from slow converters or slow decliners using the initial SPECT study. The results suggest that the initial SPECT study can discriminate between rapid decliners and slow decliners. Such discrimination is important for both therapeutic and research purposes.

Conclusion

We demonstrated that the rCBF reductions in the parietal association areas and the precunei are a good predictor of progression from MCI to AD. The data suggest that the initial rCBF SPECT in individuals with MCI could be a promising method to accurately predict who would meet diagnostic criteria for AD in the next 3 years.

Acknowledgment

This study was supported by the Promotion of Fundamental Studies in Health Science of Organization for Pharmaceuticals and Medical Devices Agency.

References

American Psychiatric Association, 1994. Diagnostic and Statistical Manual of Mental Disorders. DSM-IV (4th ed.). American Psychiatric Association, Washington, DC.

Arnaiz, E., Jelic, V., Almkvist, O., Wahlund, L.O., Winblad, B., Valind, S., et al., 2001. Impaired cerebral glucose metabolism and cognitive functioning predict deterioration in mild cognitive impairment. NeuroReport 12, 851–855.

Bruscoli, M., Lovestone, S., 2004. Is MCI really just early dementia? A systematic review of conversion studies. Int. Psychogeriatr. 16, 129–140.

Celsis, P., Agniel, A., Cardebat, D., Demonet, J.F., Ousset, P.J., Puel, M., 1997. Age related cognitive decline: a clinical entity? A longitudinal study of cerebral blood flow and memory performance. J. Neurol. Neurosurg. Psychiatry 62, 601–608.

Chetelat, G., Baron, J.C., 2003. Early diagnosis of Alzheimer's disease: contribution of structural neuroimaging. NeuroImage 18, 525–541.

Chetelat, G., Desgranges, B., de la Sayette, V., Viader, F., Eustache, F., Baron, J.C., 2003. Mild cognitive impairment: can FDG-PET predict who is to rapidly convert to Alzheimer's disease? Neurology 60, 1374–1377.

de Leon, M.J., Convit, A., Wolf, O.T., Tarshish, C.Y., DeSanti, S., Rusinek, H., et al., 2001. Prediction of cognitive decline in normal elderly subjects with 2-[(18)F]fluoro-2-deoxy-D-glucose/poitron-emission tomography (FDG/PET). Proc. Natl. Acad. Sci. U. S. A. 98, 10966–10971.

De Santi, S., de Leon, M.J., Rusinek, H., Convit, A., Tarshish, C.Y., Roche, A., et al., 2001. Hippocampal formation glucose metabolism and volume losses in MCI and AD. Neurobiol. Aging 22, 529–539.

Delacourte, A., David, J.P., Sergeant, N., Buee, L., Wattez, A., Vermersch, P., et al., 1999. The biochemical pathway of neurofibrillary degeneration in aging and Alzheimer's disease. Neurology 52, 1158–1165.

Drzezga, A., Lautenschlager, N., Siebner, H., Riemenschneider, M., Willoch, F., Minoshima, S., et al., 2003. Cerebral metabolic changes accompanying conversion of mild cognitive impairment into Alzheimer's disease: a PET follow-up study. Eur. J. Nucl. Med. Mol. Imaging 30, 1104–1113.

Folstein, M.F., Folstein, S.E., McHugh, P.R., 1975. "Mini-mental state". A practical method for grading the cognitive state of patients for the clinician. J. Psychiatr. Res. 12, 189–198.

Frisoni, G.B., Testa, C., Zorzan, A., Sabattoli, F., Beltramello, A., Soininen, H., et al., 2002. Detection of grey matter loss in mild Alzheimer's disease with voxel based morphometry. J. Neurol. Neurosurg. Psychiatry. 73, 657–664.

Hamilton, M., 1960. A rating scale for depression. J. Neurol. Neurosurg. Psychiatry 23, 56–62.

Huang, C., Wahlund, L.O., Svensson, L., Winblad, B., Julin, P., 2002. Cingulate cortex hypoperfusion predicts Alzheimer's disease in mild cognitive impairment. BMC Neurol. 2, 9.

Hughes, C.P., Berg, L., Danziger, W.L., Coben, L.A., Martin, R.L., 1982. A new clinical scale for the staging of dementia. Br. J. Psychiatry 140, 566–572.

Imabayashi, E., Matsuda, H., Asada, T., Ohnishi, T., Sakamoto, S., Nakano, S., et al., 2004. Superiority of 3-dimensional stereotactic surface projection analysis over visual inspection in discrimination of patients with very early Alzheimer's disease from controls using brain perfusion SPECT. J. Nucl. Med. 45, 1450–1457.

Jack Jr., C.R., Petersen, R.C., Xu, Y.C., O'Brien, P.C., Smith, G.E., Ivnik, R.J., 1999. Prediction of AD with MRI-based hippocampal volume in mild cognitive impairment. Neurology 52, 1397–1403.

Kogure, D., Matsuda, H., Ohnishi, T., Asada, T., Uno, M., Kunihiro, T., et al., 2000. Longitudinal evaluation of early Alzheimer's disease using brain perfusion SPECT. J. Nucl. Med. 41, 1155–1162.

Korf, E.S., Wahlund, L.O., Visser, P.J., Scheltens, P., 2004. Medial temporal lobe atrophy on MRI predicts dementia in patients with mild cognitive impairment. Neurology 63, 94–100.

McKhann, G., Drachman, D., Folstein, M., Katzman, R., Price, D., Stadlan, E.M., 1984. Clinical diagnosis of Alzheimer's disease: report of the NINCDS-ADRDA Work Group under the auspices of Department of Health and Human Services Task Force on Alzheimer's Disease. Neurology 34, 939–944.

Minoshima, S., Giordani, B., Berent, S., Frey, K.A., Foster, N.L., Kuhl, D.E., 1997. Metabolic reduction in the posterior cingulate cortex in very early Alzheimer's disease. Ann. Neurol. 42, 85–94.

Mosconi, L., Perani, D., Sorbi, S., Herholz, K., Nacmias, B., Holthoff, V., Salmon, E., Baron, J.C., De Cristofaro, M.T., Padovani, A., Borroni, B., Franceschi, M., Bracco, L., Pupi, A., 2004. MCI conversion to dementia and the APOE genotype: a prediction study with FDG-PET. Neurology 63, 2332–2340.

Mungas, D., Reed, B.R., Jagust, W.J., DeCarli, C., Mack, W.J., Kramer, J.H., et al., 2002. Volumetric MRI predicts rate of cognitive decline related to AD and cerebrovascular disease. Neurology 59, 867–873.

Nestor, P.J., Fryer, T.D., Ikeda, M., Hodges, J.R., 2003a. Retrosplenial cortex (BA 29/30) hypometabolism in mild cognitive impairment (prodromal Alzheimer's disease). Eur. J. Neurosci. 18, 2663–2667.

Nestor, P.J., Fryer, T.D., Smielewski, P., Hodges, J.R., 2003b. Limbic hypometabolism in Alzheimer's disease and mild cognitive impairment. Ann. Neurol. 54, 343–351.

Nestor, P.J., Scheltens, P., Hodges, J.R., 2004. Advances in the early detection of Alzheimer's disease. Nat. Med. 10, S34–S41 (Suppl.).

Palmer, K., Fratiglioni, L., Winblad, B., 2003. What is mild cognitive impairment? Variations in definitions and evolution of nondemented persons with cognitive impairment. Acta Neurol. Scand., Suppl. 179, 14–20.

Petersen, R.C., Doody, R., Kurz, A., Mohs, R.C., Morris, J.C., Rabins, P.V., et al., 2001a. Current concepts in mild cognitive impairment. Arch. Neurol. 58, 1985–1992.

Petersen, R.C., Stevens, J.C., Ganguli, M., Tangalos, E.G., Cummings, J.L., DeKosky, S.T., 2001b. Practice parameter: early detection of dementia: mild cognitive impairment (an evidence-based review). Report of the Quality Standards Subcommittee of the American Academy of Neurology. Neurology 56, 1133–1142.

Reiman, E.M., Chen, K., Alexander, G.E., Caselli, R.J., Bandy, D., Osborne, D., et al., 2004. Functional brain abnormalities in young adults at genetic risk for late-onset Alzheimer's dementia. Proc. Natl. Acad. Sci. U. S. A. 101, 284–289.

Talairach, J., Tournoux, P., 1988. Co-planar Stereotaxic Atlas of the Human Brain. Thieme, Stuttgart.

Available online at www.sciencedirect.com
SCIENCE DIRECT
Neuroscience Letters 395 (2006) 46–50
Neuroscience Letters
www.elsevier.com/locate/neulet

Activation of A1 and A2 noradrenergic neurons in response to running in the rat

Nao Ohiwa [a], Tsuyoshi Saito [a], Hyukki Chang [a], Takenori Omori [a], Takahiko Fujikawa [b], Takashi Asada [c], Hideaki Soya [a,*]

[a] *Laboratory of Exercise Biochemistry, University of Tsukuba, Graduate School of Comprehensive Human Sciences, 1-1-1 Tennôdai, Tsukuba, Ibaraki 305-8574, Japan*
[b] *Department of Biochemistry, Mie University School of Medicine, 2-174 Edobashi, Tsu, Mie 514-8507, Japan*
[c] *Department of Psychiatry, Institute of Clinical Medicine, University of Tsukuba, Tsukuba, Ibaraki, Japan*

Received 15 July 2005; received in revised form 14 October 2005; accepted 20 October 2005

Abstract

Since running accompanied with blood lactate accumulation stimulates the release of adrenocorticotropic hormone (ACTH), running above the lactate threshold (LT) acts as stress (running stress). To examine whether A1/A2 noradrenergic neurons that project to the hypothalamus activate under running stress, c-Fos immunohistochemistry was used to compare the effects of running with or without stress response on A1/A2 noradrenergic neurons. Blood lactate and plasma ACTH concentrations significantly increased in the running stress group, but not in the running without stress response and control groups, confirming different physiological impacts between different intensity of running with or without stress. Running stress markedly increased c-Fos accumulation in the A1/A2 noradrenergic neurons. Running without stress response also induced a significant increase in c-Fos expression in the A1/A2 noradrenergic neurons, and the percentage of the increase was smaller than that of running stress. The extent of c-Fos expression in the A1/A2 noradrenergic neurons correlates with exercise intensity, signifying that this neuronal activation is running speed-dependent. We thus suggest that A1/A2 noradrenergic neurons are activated in response to not only running stress, but also to other physiological running, enhanced by non-stressful running. These findings will be helpful in studies of specific neurocircuits and in identifying their functions in response to running at different intensities.

Keywords: A1/A2; Running stress; Noradrenaline; Hypothalamic paraventricular nucleus; Lactate threshold; Rat

Exercise at around the lactate threshold (LT) produces a variety of physiological and psychological effects on the body [13,26] and thus it has been widely used as a beneficial tool for preventing or ameliorating lifestyle-related diseases in the clinical field. However, the effects of this intensity of exercise on brain function have yet to be determined. The LT is a work rate at which the steady state of blood lactate accumulation breaks down [28] and the plasma adrenocorticotropic hormone concentration begins to increase notably during graded running [6,12,18]. Since it is well known that ACTH release is a marker of stress [15], acute running can act as one kind of stress, termed running stress, if it persists above the LT. We would like to know what brain regulatory mechanisms underlie running stress just above the LT since it would add greatly to our understanding of the mechanisms behind the variety of physio-/psychological benefits produced by exercise around the LT.

Little is known about the regulating mechanism underlying running stress, although we have previously delineated anatomical activation of the parvocellular part of the hypothalamic paraventricular nucleus (pPVN) during running stress using our rat treadmill running model [20,25]. We further attempted to determine the nuclei or neuropeptides that regulate ACTH release during running stress via pPVN activation. The A1 and the A2 noradrenergic (NA) neurons that project to the pPVN are prime candidates for the regulation of running stress, since these noradrenergic neurons play a crucial role in other ACTH releases induced by stress, such as hypoxia [23], hemorrhage [3] and swimming stress [22]. However, it is very odd that no one has examined whether NA neurons in the A1/A2 are responsive to running stress, despite considerable physiological changes

* Corresponding author. Tel.: +81 29 853 2620; fax: +81 29 853 2620.
E-mail address: hsoya@taiiku.tsukuba.ac.jp (H. Soya).

0304-3940/$ – see front matter © 2005 Elsevier Ireland Ltd. All rights reserved.
doi:10.1016/j.neulet.2005.10.053